

# Macromodeling of Parabolic Double Negative Metamaterial Antennas

By Grzegorz Lubkowski, Franz Hirtenfelder, Bastian Bandlow, Rolf Schuhmann and Thomas Weiland

**Abstract** – The paper presents a methodology for the modeling of metamaterial structures which are built as lattices of double negative unit cells. The effective description for a double negative unit cell is found by parameter fitting of dispersive models. The obtained models are implemented in higher level simulations and used for the characterization of large metamaterial macrostructures. A parabolic antenna composed of split ring resonators and wires is analyzed by this approach, and its radiation and refraction behavior is evaluated. The simulation results for the detailed and effective representations of the antenna are compared to each other and validate the proposed modeling approach.

**Index Terms** – Metamaterials, Antennas, Negative Refraction

## 1. Introduction

During a few recent years, artificial media with negative real parts of the electric permittivity and magnetic permeability (hence DNG: double negative materials) gained enormous interest in the scientific community [1, 2, 3]. The unconventional, not available in nature response functions of these structures are generated by artificially fabricated inclusions or inhomogeneities embedded in a host medium. One of the most popular concepts for the construction of a double negative metamaterial cell is to use a combination of a split ring resonator (SRR) and a wire, providing frequency dependent negative magnetic permeability and negative electric permittivity, respectively [4].

Metamaterial (MTM) structures are built of periodically ordered cells, with the assumption that the lattice constant is much shorter than the wavelength in the medium. A DNG unit cell typically contains very fine elements (e.g. narrow gaps in split ring resonators, thin metal wires) in its structure. Consequently, the details of the structure are very small with respect to the wavelength, which makes it challenging to include them in the full-wave 3D electromagnetic analysis. On the other hand, the observation of the desirable macro-effects (e.g. negative refraction) requires that the MTM should have the size of at least several wavelengths. The number of unit cells in a 2D MTM medium (e.g. one layer DNG lattice) is typically of the order of 100.

When both micro- and macro- requirements are combined, one ends up with the computationally large problem which renders the numerical analysis impractical. To make the simulation of the macro-effects virtually possible, one describes a DNG structure by the effective parameters, i.e. effective electric permittivity and effective magnetic permeability. Effective parameters are typically obtained from the simulation of metamaterial unit cells. The electromagnetic behavior of

the effective macrostructure should be equivalent to the corresponding results for the detailed model.

The main aim of this work is to present a modeling approach applied to MTM structures, based on an example of a DNG MTM parabolic antenna. The MTM is simulated at two levels: as a microstructure (single unit cell), or macrostructure (periodic lattice) [5, 6]. First, at the microstructure level, the effective material parameters are extracted from the results of 3D field simulations in a single unit cell, i.e. from its scattering matrix. The effective parameters are computed by the parameter fitting of dispersive models. Next, the equivalent representation of the MTM macrostructure is formed as a properly shaped homogeneous slab described by the extracted and optimised dispersive Drude and Lorentz models. Finally, the MTM macrostructure is simulated as the effective structure as well as the detailed lattice, and the corresponding numerical results are compared. All simulations are performed using a commercial implementation of the Finite Integration Technique, FIT [7], i.e. with the software package CST Microwave Studio (MWS) [8].

## 2. Extraction of Effective Material Parameters

There are several methods for the extraction of effective material parameters for DNG MTM structures. The most popular approach is the extraction from transmission and reflection characteristics, the method commonly used to find the effective parameters of a material sample under test by the experimental measurement of its scattering matrix [9]. Several variations of this approach applied to MTM are presented in [10, 11, 12].

In the frame of this work, the method based on parameter fitting of dispersive models (PFDM) is used [13]. The effective material parameters are found by fitting scattering parameters of the equivalent homogeneous representation to the  $S$  matrix of the reference structure. The reference structure is a detailed DNG geometry simulated in the electromagnetic solver, whereas the effective representation is a slab of an isotropic, homogeneous material described by dispersive Drude (electric permittivity) and Lorentz (magnetic permeability) models. The coefficients of the dispersive models are the parameters in the optimization process. The optimization goal is to minimize the difference between the scattering parameters obtained for the reference structure and the homogeneous structure. The homogeneous cell should provide the same transmission/reflection behavior as the SRR/wire based DNG cell.

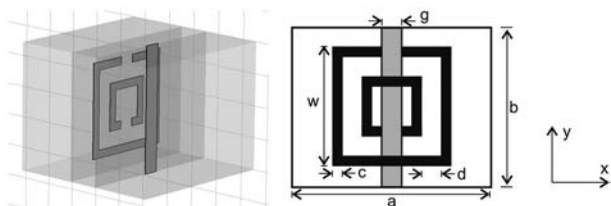


Fig. 1: The DNG MTM unit cell. LHS: MWS implementation of the SRR/wire reference unit cell; RHS: unit cell dimensions: gap width  $g = 0.5$  mm, wire width  $g = 0.5$  mm, lattice constant  $a = 5$  mm, cell height  $b = 4$  mm, outer SRR height  $w = 3$  mm, ring spacing  $d = 0.5$  mm, strip width  $c = 0.25$  mm.

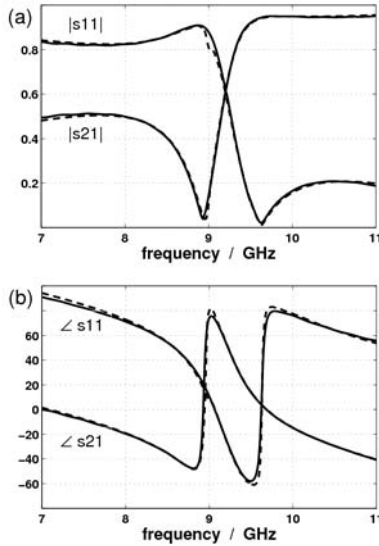


Fig. 2: Magnitude (a) and angle (in deg, b) of scattering parameters for SRR/wire reference structure (solid line) and for the optimized homogeneous structure (dashed line).

The simulation procedure for the DNG reference cell (Fig. 1) is similar to the one used in [14] and described in detail in [13]. An automeshing algorithm is used in MWS to create the computational grid for the SRR/wire geometry. The structure is simulated with the time-domain solver, the excitation pulse has a Gaussian distribution in time domain that is transformed into 1000 intermediate frequencies from 7 to 11 GHz in the frequency domain. Magnetic boundary conditions are applied at the faces along the axis of the rings ( $\pm z$  limits) and electric boundary conditions are used at the  $\pm y$  faces of the mesh volume. The ports are at the  $\pm x$  limits of the mesh volume where open boundary conditions are used. The structure is excited by the first mode of a so-called waveguide port, with the electric field of a plane wave polarized in the  $y$  direction and propagating along the  $x$  direction. The ring and the wire are simulated as copper and placed on a 1 mm thick dielectric slab characterized by  $\epsilon_R = 3.4$ . Obtained reference scattering parameters are presented in Fig. 2.

The effective representation of the DNG MTM cell is a homogeneous slab with the same unit cell dimensions as the MTM unit cell. The scattering parameters for the homogenized DNG cell are obtained analytically. The effective permittivity and permeability models are assumed to be of Drude and Lorentz form, respectively (the values of  $\epsilon_{\text{eff}}$  and  $\mu_{\text{eff}}$  are relative to those in free space):

$$\epsilon_{\text{eff}}(\omega) = \epsilon_{\infty} - \frac{\omega_p^2}{\omega(\omega - i\nu_c)} \quad (1)$$

where  $\epsilon_{\infty}$  electric permittivity at the high frequency limit,  $\omega_p$  radial plasma frequency,  $\nu_c$  collision frequency;

$$\mu_{\text{eff}}(\omega) = \mu_{\infty} + \frac{(\mu_s - \mu_{\infty})\omega_0^2}{\omega_0^2 + i\omega\delta - \omega^2} \quad (2)$$

where  $\mu_s/\mu_{\infty}$  magnetic permeability at the low/high frequency limit,  $\omega_0$  radial resonant frequency,  $\delta$  damping frequency.

An optimization algorithm [15] searches for the values of  $\epsilon_{\text{eff}}$  and  $\mu_{\text{eff}}$  subparameters (i. e.:  $\epsilon_{\infty}$ ,  $\omega_p$ ,  $\nu_c$ ,  $\mu_s$ ,  $\mu_{\infty}$ ,  $\omega_0$ ,  $\delta$ ) providing the best fit between the scattering parameters of the homogenized ( $S_{11}$ ,  $S_{21}$ ) and the reference structure ( $S_{11_{\text{ref}}}$ ,  $S_{21_{\text{ref}}}$ ). The optimizer goal function takes the form:

$$G = \sum_i (|S_{11} - S_{11_{\text{ref}}}|_{\text{fit}} + |S_{21} - S_{21_{\text{ref}}}|_{\text{fit}}) \quad (3)$$

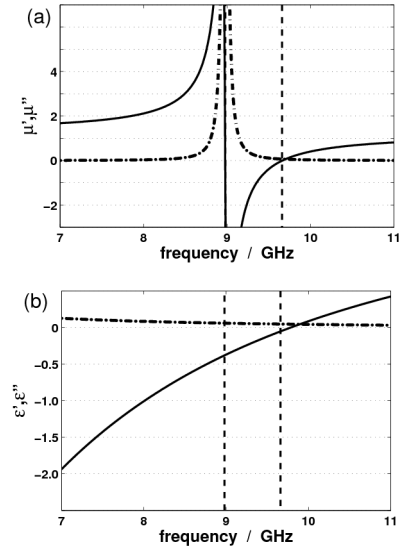


Fig. 3: Effective magnetic permeability  $\mu_{\text{eff}} = \mu' - j\mu''$  (a) and electric permittivity  $\epsilon_{\text{eff}} = \epsilon' - j\epsilon''$  (b) obtained by parameter fitting of dispersive models ( $\mu'$ ,  $\epsilon'$  solid line,  $\mu''$ ,  $\epsilon''$  dash-dot line); the dashed vertical lines limit the DNG frequency band (9–9.65 GHz).

where scattering parameters are fitted at  $i$  frequencies in the frequency range of interest.

The optimized parameters of Drude and Lorentz models for the structure in Fig. 1 are given in Tab. 1. A comparison of magnitude and angle of scattering parameters obtained by optimization with the reference results in Fig. 2 shows a very good fitting. Corresponding  $\epsilon_{\text{eff}}$  and  $\mu_{\text{eff}}$  characteristics given in Fig. 3 show a DNG behavior in the frequency range 9–9.65 GHz. The delivered dispersive models form the effective description for the homogeneous model of the MTM macrostructure.

<unbekanntes object>

In the analysed frequency band (7–11 GHz) four frequency regions can be distinguished [5]. The first region (7–9 GHz) is the single negative band (SNG,  $\epsilon_{\text{eff}} < 0$  and  $\mu_{\text{eff}} > 0$ ) characterized by high attenuation and very weak transmission. The second region (9–9.65 GHz) is the double negative band (DNG,  $\epsilon_{\text{eff}} < 0$  and  $\mu_{\text{eff}} < 0$ ), where unusual phenomena (e. g. negative refraction) can be observed. The narrow third frequency band (9.65–9.8 GHz) is similar to the first one a SNG stopband ( $\epsilon_{\text{eff}} < 0$  and  $\mu_{\text{eff}} > 0$ ). Finally, the fourth region (9.8–11 GHz) is the double positive band (DPS,  $\epsilon_{\text{eff}} > 0$  and  $\mu_{\text{eff}} > 0$ ), where common phenomena (e. g. positive refraction) occur.

### 3. Macrostructure Simulations

The MTM macrostructure analysed in this paper is a MTM lattice of a parabolic shape, which due to its DNG properties leads to an unusual phenomenon [16]. With a negative index of refraction, the refracted wave occurs on the same side of the normal to the boundary as the incident wave, which leads to the focusing of waves in the DNG frequency range. The detailed implementation of the single MTM layer is built of 125

Table 1: Optimized Drude/Lorentz parameters for DNG MTM structure.

Parameter	Optimized Value
$\epsilon_{\infty}$	2.03
$\omega_p$	$2 \cdot \pi \cdot 13.96$ GHz
$\nu_c$	1.407 GHz
$\mu_s$	1.38
$\mu_{\infty}$	1.19
$\omega_0$	$2 \cdot \pi \cdot 8.98$ GHz
$\delta$	0.453 GHz

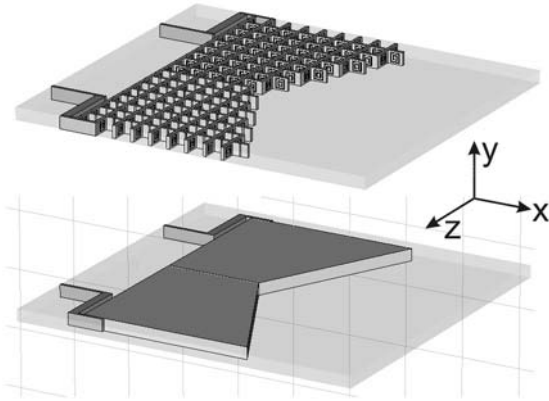


Fig. 4: Detailed (top) and effective (bottom) representation of the plane-concave MTM lens.

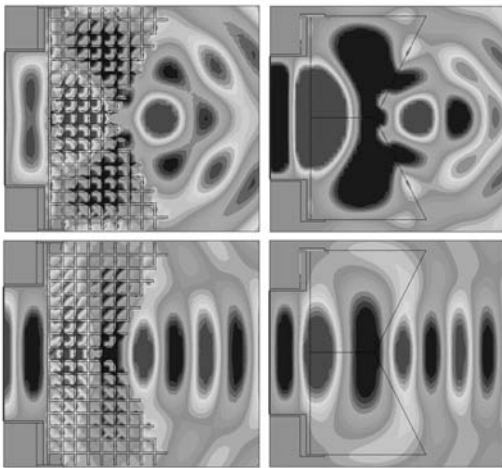


Fig. 5: Distribution of the electric field ( $xz$  plane) in the DNG (9.3 GHz, top) and DPS (11 GHz, bottom) frequency range for the detailed (LHS) and effective (RHS) representation of the MTM macrostructure. .

SRR/wire unit cells, periodically repeated with the lattice constant  $a = 5$  mm in  $x$  and  $z$  directions (Fig. 4, top). The macrostructure shape forms a plane-concave type lens. When built of a typical double positive (DPS) material, i.e. characterised by both positive electric permittivity and magnetic permeability, the plane-concave lens has diverging properties.

The effective model of the MTM macrostructure (Fig. 4, bottom) is a homogenous slab with the shape and dimensions corresponding to the detailed MTM lattice. Its constitutive parameters are described by the frequency dependent Drude and Lorentz models summarized in Table 1.

Both structures are simulated with the time-domain MWS solver, which allows to evaluate the distribution of the electromagnetic fields at frequencies of interest in one transient run due to the recorded field monitors based on discrete Fourier transform. The structure is excited from the waveguide port at the  $-x$  face,  $E_y$  field polarization, wave propagation in  $+x$  direction). A very good agreement between the corresponding field patterns for the detailed (LHS) and effective (RHS) macrostructures can be noticed.

The predicted focusing behavior in the DNG frequency range (9.3 GHz) and the lack thereof in the DPS frequency range (11 GHz) is demonstrated in Fig. 5. The figure presents the distribution of the electric field for a plane wave excitation from the left hand side (LHS) of the structure (waveguide port at the  $-x$  face,  $E_y$  field polarization, wave propagation in  $+x$  direction). A very good agreement between the corresponding field patterns for the detailed (LHS) and effective (RHS) macrostructures can be noticed.

To further demonstrate the focusing properties of the structure, the spatial distribution of the normalized electric

field in the  $yz$  plane on the right hand side (RHS) of the lens is presented in Fig. 6. The  $z = 0$  plane corresponds to the symmetry axis of the macrostructure.

The strong focusing effect can be noticed in the frequency range of double negative parameters. This effect is lost while approaching the double positive range above 10 GHz. A very good qualitative agreement between the field distributions for the effective and detailed macrostructures can be noticed (also at 12 GHz, i.e. at the frequency out of the validity range of the Drude/Lorentz description). According to the predictions from the unit cell analysis (Section 2) a strong attenuation (of the order of 50 dB) for the signal transmitted through the lens is observed below 9 GHz, due to the single negative material parameters in this range (field distributions not shown here). The absolute values of magnitude for the transmitted electric field are comparable in the DNG and DPS frequency ranges (i.e. there are no significant losses in the DNG frequency band). The absolute values of the field magnitude for the detailed and effective macrostructures are also of the same order (note that the normalized values are reported in Fig. 6).

The layers of the investigated MTM structure can be stacked in the vertical dimension and act as a type of antenna, with its farfield characteristics predicted by numerical simulations.

In Fig. 7 the 4-layer detailed MTM structure and the corresponding farfield characteristic are presented. The number of MTM unit cells in this case is of the order of 500 and the numerical costs of the simulations are tremendous. The simulated phase center for the detailed structure at the frequency of 9.45 GHz is located 42 mm from the lens face.

The numerical costs can be significantly reduced by simulation of the equivalent effective structure characterized by the extracted Drude/Lorentz models. The corresponding homogeneous macrostructure and its farfield characteristic is presented in Fig. 8. The computed phase center is located 41.2 mm from the slab face. This value is in a very good

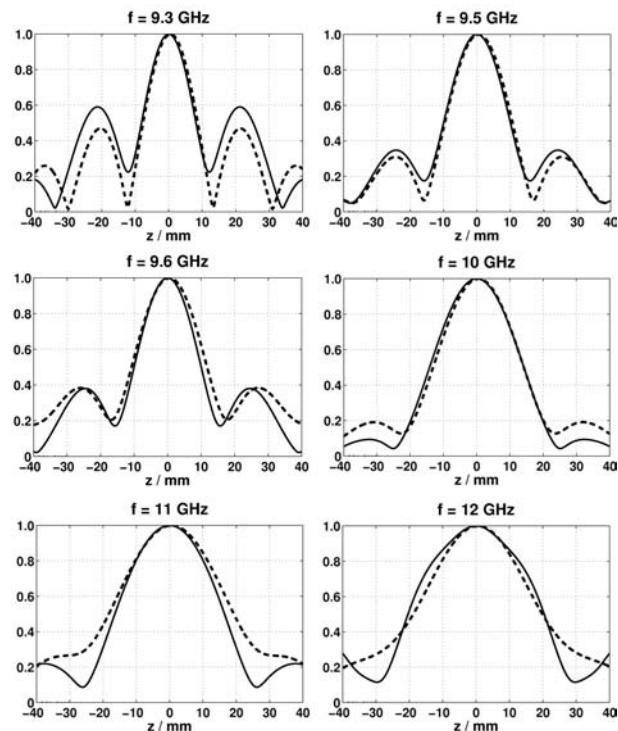


Fig. 6: Distribution of the normalized electric field on the RHS of the focusing MTM lens at 3 frequencies in the DNG range (9.3, 9.5, 9.6 GHz) and at 3 frequencies in the DPS range (10, 11, 12 GHz): solid line – detailed macrostructure, dashed line – effective macrostructure. Fig. 5: Distribution of the electric field ( $xz$  plane) in the DNG (9.3 GHz, top) and DPS (11 GHz, bottom) frequency range for the detailed (LHS) and effective (RHS) representation of the MTM macrostructure. .

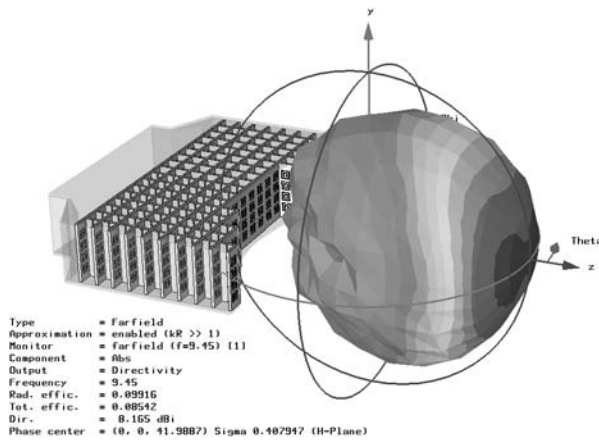


Fig. 7: Farfield directivity of the SRR/wire composite antenna with the computed phase center at 42 mm.

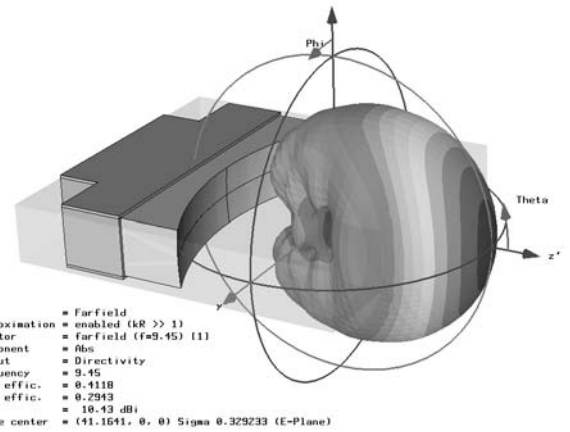


Fig. 8: Farfield directivity of the effective bulk antenna with the computed phase center at 42 mm.

agreement with the reference phase center location obtained for the detailed lens in Fig. 7.

The presented effective models allow for a substantial reduction of computational costs, typically of 2 orders of magnitude (i. e. by a factor of 100) regarding the memory as well as CPU requirements. Numerical analysis with the time-domain solver deliver all important quantities such as field monitors and farfield characteristics within one transient simulation run.

#### 4. Conclusions

A numerical approach to the modeling of metamaterial structures is presented based on the example of a parabolic metamaterial antenna. Starting with the numerical analysis of a single unit cell, effective material parameters are obtained by parameter fitting of dispersive models. The resulting models form the effective description of the metamaterial and allow to predict its macroscopic behavior. The effective macromodels allow for substantial savings of computational costs regarding 3D full-wave numerical analysis of metamaterials. A very good agreement between the simulation results of the detailed and effective structure validates the proposed macromodeling approach.

#### References

- [1] R.W. Ziolkowski, N. Engheta (editors), Special Issue on Metamaterials, *IEEE Trans Antennas Propag*, vol. 51, no. 10, pp. 2546–2750, 2003.
- [2] T. Itoh, A.A. Oliner (editors), Special Issue on Metematerials, *IEEE Trans Microwave Theory Tech*, vol. 53, no. 4, pp. 1413–1556, 2005.
- [3] G. Eleftheriades, Y. Vardaxoglou (editors), Special Issue on Metamaterials, *IET Microwaves, Antennas And Propagation*, vol. 1, no. 1, pp. 1–266, 2007.
- [4] R.A. Shelby, D.R. Smith, S. Schultz, “Experimental Verification of a Negative Index of Refraction”, *Science*, vol. 292, pp. 77–79, 2001.
- [5] G. Lubkowski, F. Hirtenfelder, R. Schuhmann, T. Weiland, “3D Full-wave Field Simulations of Double Negative Metamaterial Macrostructures”, *Proceedings of Metamaterials 2007 Conference*, Rome, pp. 731–734, 22–24 October 2007.
- [6] R. Schuhmann, B. Bandlow, G. Lubkowski, T. Weiland, “Micro- and Macroscopic Simulation of Periodic Metamaterials”, *submitted to Advances in Radio Science*, 2008.
- [7] T. Weiland, “A Discretization Method for the Solution of Maxwell’s Equations for Six-Components”, *AEÜ International Journal of Electronics and Communications*, vol. 31, pp. 116–120, 1977.
- [8] Computer Simulation Technology, CST, <http://www.cst.com>.
- [9] A.M. Nicolson, G.F. Ross, “Measurement of the Intrinsic Properties of Materials by Time-Domain Techniques”, *IEEE Trans Instrum Meas*, vol. 19, pp. 377–382, 1970.

- [10] R.W. Ziolkowski, “Design, Fabrication and Testing of Double Negative Metamaterials”, *IEEE Trans Antennas Propag*, vol. 51, pp. 1516–1529, 2003.
- [11] D.R. Smith, S. Schultz, P. Markos, C.M. Soukoulis, “Determination of Effective Permittivity and Permeability of Metamaterials from Reflection and Transmission Coefficients”, *Physical Review B*, vol. 65, pp. 195104, 2002.
- [12] P. Markos, C.M. Soukoulis, “Transmission Properties and Effective Electromagnetic Parameters of Double Negative Metamaterials”, *Opt Express*, vol. 11, pp. 649–661, 2003.
- [13] G. Lubkowski, R. Schuhmann, T. Weiland, “Extraction of Effective Metamaterials Parameters by Parameter Fitting of Dispersive Models”, *Microwave and Optical Technology Letters*, vol. 49, no. 2, pp. 285–288, 2007.
- [14] T. Weiland, R. Schuhmann, R.B. Gregor, C.G. Parazzoli, A.M. Vetter, D.R. Smith, D.C. Vier, S. Schultz, “Ab initio Numerical Simulation of Left-handed Metamaterials: Comparison of Calculations and Experiments”, *Journal of Applied Physics*, vol. 90, no. 10, pp. 5419–5424, 2001.
- [15] R. Storn, K. Price, “Differential Evolution – a Simple and Efficient Heuristic for Global Optimization over Continuous Spaces”, *Journal of Global Optimization*, vol. 11, pp. 341–359, 1997.
- [16] F. Hirtenfelder, G. Lubkowski, “3D Field Simulations using FI Time Domain Technique of Wedge- and Parabolic-Shaped Left Handed Materials”, *Proceedings of Int Workshop on Small and Smart Antennas, Metamaterials and Applications iWAT07*, Cambridge, U.K., pp. 259–262, 21–23 March 2007.

This work was supported by DFG (GRK 1037/1–04)

Grzegorz Lubkowski  
Thomas Weiland  
Institut für Theorie Elektromagnetischer Felder  
Technische Universität Darmstadt  
Schloßgartenstraße 8  
64289 Darmstadt  
Germany  
Fax: +49-6151-164611  
E-mail: lubkowski@temf.de

Franz Hirtenfelder  
CST GmbH  
Bad Nauheimer Strasse 19  
64289 Darmstadt  
Germany

Bastian Bandlow  
Rolf Schuhmann  
EIM-E Fachgebiet Theoretische Elektrotechnik  
Universität Paderborn  
Warburger Straße 100  
33098 Paderborn  
Germany

(Received on February 22, 2008)  
(Revised on March 25, 2008)